

# Potassium *tert*-Butoxide-Catalyzed Dehydrogenative C–H Silylation of Heteroaromatics: A Combined Experimental and Computational Mechanistic Study

Wen-Bo Liu,<sup>†,#</sup> David P. Schuman,<sup>†,#</sup> Yun-Fang Yang,<sup>‡,#,Ⓛ</sup> Anton A. Toutov,<sup>†</sup> Yong Liang,<sup>‡</sup> Hendrik F. T. Klare,<sup>Ⓛ</sup> Nasri Nesnas,<sup>§</sup> Martin Oestreich,<sup>Ⓛ</sup> Donna G. Blackmond,<sup>∇</sup> Scott C. Virgil,<sup>†</sup> Shibdas Banerjee,<sup>||</sup> Richard N. Zare,<sup>||</sup> Robert H. Grubbs,<sup>†</sup> K. N. Houk,<sup>\*,‡,Ⓛ</sup> and Brian M. Stoltz<sup>\*,†,Ⓛ</sup>

<sup>†</sup>Division of Chemistry and Chemical Engineering, California Institute of Technology, Pasadena, California 91125, United States

<sup>‡</sup>Department of Chemistry and Biochemistry, University of California, Los Angeles, California 90095, United States

<sup>Ⓛ</sup>Institut für Chemie, Technische Universität Berlin, Strasse des 17. Juni 115, 10623 Berlin, Germany

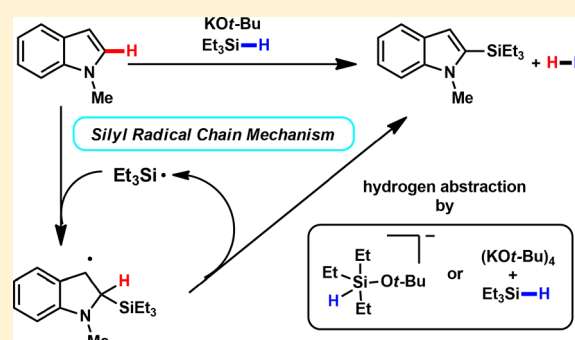
<sup>§</sup>Department of Chemistry, Florida Institute of Technology, 150 West University Boulevard, Melbourne, Florida 32901, United States

<sup>||</sup>Department of Chemistry, Stanford University, Stanford, California 94305, United States

<sup>∇</sup>Department of Chemistry, The Scripps Research Institute, La Jolla, California 92037, United States

## Supporting Information

**ABSTRACT:** We recently reported a new method for the direct dehydrogenative C–H silylation of heteroaromatics utilizing Earth-abundant potassium *tert*-butoxide. Herein we report a systematic experimental and computational mechanistic investigation of this transformation. Our experimental results are consistent with a radical chain mechanism. A trialkylsilyl radical may be initially generated by homolytic cleavage of a weakened Si–H bond of a hypercoordinated silicon species as detected by IR, or by traces of oxygen which can generate a reactive peroxide by reaction with [KO*t*-Bu]<sub>4</sub> as indicated by density functional theory (DFT) calculations. Radical clock and kinetic isotope experiments support a mechanism in which the C–Si bond is formed through silyl radical addition to the heterocycle followed by subsequent β-hydrogen scission. DFT calculations reveal a reasonable energy profile for a radical mechanism and support the experimentally observed regioselectivity. The silylation reaction is shown to be reversible, with an equilibrium favoring products due to the generation of H<sub>2</sub> gas. In situ NMR experiments with deuterated substrates show that H<sub>2</sub> is formed by a cross-dehydrogenative mechanism. The stereochemical course at the silicon center was investigated utilizing a <sup>2</sup>H-labeled silolane probe; complete scrambling at the silicon center was observed, consistent with a number of possible radical intermediates or hypercoordinate silicates.



## INTRODUCTION

Heteroarenes are important components of natural products and bioactive molecules, and considerable research has focused on their functionalization and derivatization.<sup>1</sup> Direct functionalization of unactivated C–H bonds in heteroarenes is a powerful method to access heteroarylsilanes and heteroarylboranes.<sup>2</sup> These intermediates provide routes to build complexity in molecules by well-established cross-coupling techniques.<sup>3</sup> Heteroarylsilanes are stable and find widespread use in polymer synthesis, medical imaging applications, and drug discovery.<sup>4</sup> Given the diversity and abundance of both heteroarenes and hydrosilanes, direct C–H silylation between heteroarenes and hydrosilanes is a powerful tool for the selective construction of C–Si bonds.<sup>5,6</sup> In comparison with traditional methods (i.e., metalation/nucleophile trapping), direct cross-dehydrogenative C–H silylation constitutes an appealing alternative without requiring prefunctionalization of

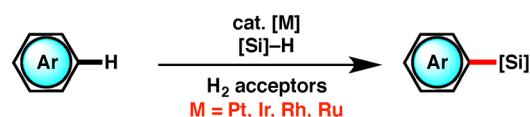
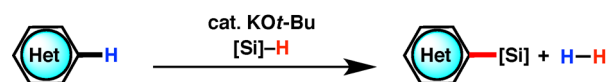
the heteroarene, cryogenic conditions, or pyrophoric reagents.<sup>7</sup> Significant advances in this field include the development of Ir/Rh catalysts that efficiently enable C–H silylation of heteroarenes in the presence of superstoichiometric sacrificial hydrogen acceptors (Scheme 1a) and more recent examples of catalytic Friedel–Crafts silylation of arenes.<sup>6,8,9</sup> Given the state of the art in C–H silylation, we sought a practical, sustainable, and scalable silylation method achieving efficient silylation of a broad scope of substrates. We have demonstrated that potassium *tert*-butoxide (KO*t*-Bu) alone can catalyze the direct cross-dehydrogenative coupling of heteroarenes with hydrosilanes (Scheme 1b).<sup>10</sup> This method features mild reaction conditions, an operationally simple procedure, good functional group tolerance, and environmentally friendly

Received: December 19, 2016

Published: April 12, 2017

## Scheme 1. Synthesis of Heteroarylsilanes by Catalytic Direct C–H Silylations

## (a) Previous Transition-Metal-Catalyzed C–H Silylation Work

(b) KO $t$ -Bu-Catalyzed Cross-Dehydrogenative C–H Silylation Method

reagents. However, the mechanism by which this reaction occurs is not obvious and has driven a broad collaborative study toward gaining insight into the reaction, described in both this and the [accompanying paper](#).<sup>11</sup> Herein we report a collection of evidence consistent with a radical mechanism, indicated by both experimental and computational mechanistic investigations. The companion publication describes an ionic and neutral mechanism for this reaction.

## ■ COMPUTATIONAL DETAILS

Calculations were carried out with Gaussian 09.<sup>12</sup> Geometry optimizations and energy calculations were performed with the B3LYP and UB3LYP (for radical species) method.<sup>13</sup> The 6-31G (d) basis set was used for all atoms.<sup>14</sup> Frequency analysis verified the stationary points are minima or saddle points. Single-point energies were calculated at the M062X (UM062X) /6-311+G(d,p) level.<sup>15</sup> Solvent effect (solvent = THF) was calculated by using CPCM solvation model.<sup>16</sup>

## ■ RESULTS AND DISCUSSION

**Effect of Catalyst Identity.** We have previously reported that the combination of a bulky basic anion and a potassium cation is crucial for the C–H silylation of 1-methylindole.<sup>10</sup> A detailed study of the catalytic competency of a variety of alkali, alkaline earth, and other metal-derived bases has been conducted. As shown in [Table 1](#), alkoxides and hydroxides of alkali metals with larger radius cations (i.e., radius  $\geq K^+$ ), such as  $K^+$ ,  $Rb^+$ , and  $Cs^+$ , could provide the silylation product in moderate to good yields ([Table 1](#), entries 1–4, 6, 9, and 10). Among all the catalysts examined, KO $t$ -Bu was proven to be the ideal catalyst, affording the highest overall yield. However, no product was detected when KOAc or KH was employed as the catalyst (entries 5 and 7). Perhaps surprisingly, potassium on graphite ( $KC_8$ ) afforded the desired product in good yield (entry 8). Alkali metal bases with small cations (e.g., LiO $t$ -Bu and NaO $t$ -Bu) demonstrated a complete lack of reactivity, and no product was observed even after extended reaction time (entries 11 and 12). Alkoxides of alkali earth metals or aluminum were also investigated as catalysts and failed to afford any product (entries 13–16).

The kinetic behavior of the silylation reaction with KO $t$ -Bu catalyst was studied using in situ  $^1H$  NMR spectroscopy. As depicted in [Figure 1](#), the silylation reaction was found to take place in three stages: an induction period ([Figure 1](#), 0–3500 s), an active period with rapid formation of product (3500–4500 s),<sup>18</sup> and a final period with significantly reduced reaction rate (>4500 s). Our investigations were then expanded to include each active catalyst presented in [Table 1](#) ([Figure 2](#)). The length of the induction period was found to depend on the nature of both metal and counterion. For anions, the induction period

Table 1. Evaluation of Base Metal Catalyst<sup>a</sup>

entry	catalyst	time (h)	conv (%) <sup>b</sup>	2:3 <sup>b</sup>
1	KO $t$ -Bu	10	88	11:1
2	KOEt	10	55	9:1
3	KOMe	20	35	9:1
4	KOTMS	20	53	12:1
5	KOAc	60	0	
6	KOH <sup>c,e</sup>	20	52	11:1
7	KH	36	0	
8	$KC_8$ <sup>d</sup>	10	73	8:1
9	$CsOH \cdot H_2O$ <sup>e</sup>	10	64	8:1
10	$RbOH \cdot xH_2O$ <sup>e</sup>	10	38	10:1
11	LiO $t$ -Bu	36	0	
12	NaO $t$ -Bu	36	0	
13	$Mg(Oi-Pr)_2$	36	0	
14	$Ca(Oi-Pr)_2$	36	0	
15	$Ba(Oi-Pr)_2$	36	0	
16	$Al(Oi-Pr)_3$	36	0	

<sup>a</sup>Reaction conditions: **1** (0.5 mmol),  $Et_3SiH$  (1.5 mmol), and catalyst (0.1 mmol, 20 mol%) in THF (0.5 mL) at 45 °C. <sup>b</sup>Determined by GC analyses. <sup>c</sup>Dried KOH; see [Supporting Information](#) for details. <sup>d</sup>Potassium graphite. <sup>e</sup>The hydroxides may be converted to silanolates, and subsequently silicates, which serve as the active catalysts under the reaction conditions.<sup>17</sup>

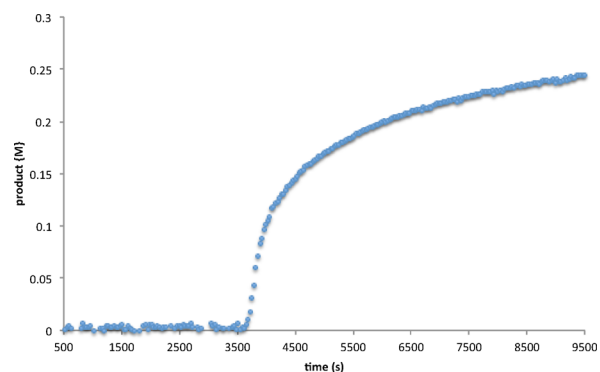


**Figure 1.** Representative time course of the silylation of **1**, monitored by in situ  $^1H$  NMR. Reaction conditions: **1** (0.25 mmol),  $Et_3SiH$  (0.75 mmol), and KO $t$ -Bu (0.05 mmol, 20 mol%) in THF- $D_8$  (0.25 mL) at 45 °C in a sealed NMR tube.

increased in the order of  $KC_8$  (shortest) < KOEt < KO $t$ -Bu < KOH (longest). An increase in induction period was observed with decreasing radius of cations, with  $CsOH$  (shortest) <  $RbOH$  < KOH (longest).<sup>19</sup> It is worth noting that the induction periods vary based on catalyst loading, solvents, and reaction temperature. Additives and moisture could also have a significant impact on the induction period, generally prolonging the duration of such period (see [Supporting Information \(SI\)](#)). Nevertheless, the induction period showed good reproducibility for identical reactions set up at different times. Although the induction period with KO $t$ -Bu is not the shortest for all catalysts tested ([Figure 2](#)), this catalyst provides the highest post-initiation turnover frequency and product yield. Further

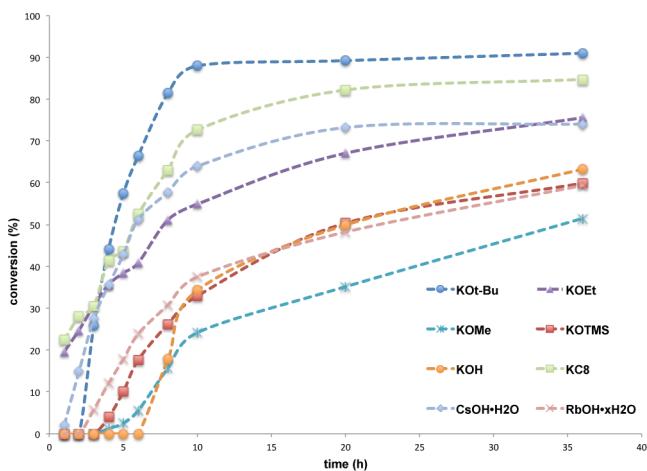


**Figure 2.** Comparison of the kinetic profiles of multiple base catalysts. Data were acquired via GC analysis of aliquots of crude reaction mixture.

discussion related to the cause of this induction period is explored in later spectroscopic and computational experiments.

**Regioselectivity and Reversibility.** Although the major product of *KOt*-Bu-catalyzed silylation results from the incorporation of a triethylsilyl group at the C2 position of 1-methylindole (**2**), C3-silylation product **3** is also formed. Increase in reaction time and temperature tends to shift the major product from C2- to C3-silylation. As illustrated in Table 2, the reaction in THF at 45 °C affords an 11:1 ratio of C2:C3

**Table 2. Regioselectivity as a Function of Reaction Conditions<sup>a</sup>**

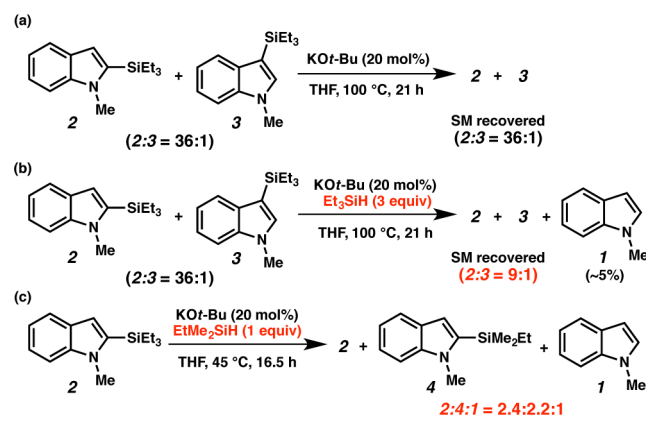
entry	solvent	temp (°C)	time (h)	conv (%) <sup>b</sup>	2:3 <sup>b</sup>
1	THF	45	10	88	11:1
2	THF	45	— <sup>c</sup>	>95	1:>20
3	THF	100	20	94	1:9
4	neat	45	48	88	>20:1
5	neat	100	24	>95	4:1

<sup>a</sup>Reaction conditions: **1** (0.5 mmol), Et<sub>3</sub>SiH (1.5 mmol), and *KOt*-Bu (0.1 mmol, 20 mol%) in THF (0.5 mL, if indicated). <sup>b</sup>Determined by GC analyses. <sup>c</sup>After 15 days.

products (**2**:**3**) after 10 h, but after 15 days under the same conditions only C3 product **3** is observed (i.e., 1:>20 C2:C3, entries 1 and 2). Similarly, when the reaction is conducted at 100 °C, C3-silylation predominates with a 1:9 ratio of products **2**:**3** (entry 3). These results are consistent with C2-silylation as the kinetic product, while C3-silylation is the thermodynamic product. Finally, solvent selection was found to have a dramatic impact on the C2 and C3 selectivity. In the absence of solvent, the C2 product is exclusively observed at 45 °C, and even at 100 °C, C2-silylation is still the major pathway (entries 4 and 5).

Several experiments were conducted to probe the reversibility of the silylation reaction (Scheme 2). Treatment of C2-silylated compound **2** with *KOt*-Bu in THF does not result in conversion to the C3-silylated **3** (Scheme 2a), showing that catalyst alone is insufficient for reversibility. However, treat-

**Scheme 2. Reversibility of the Silylation**

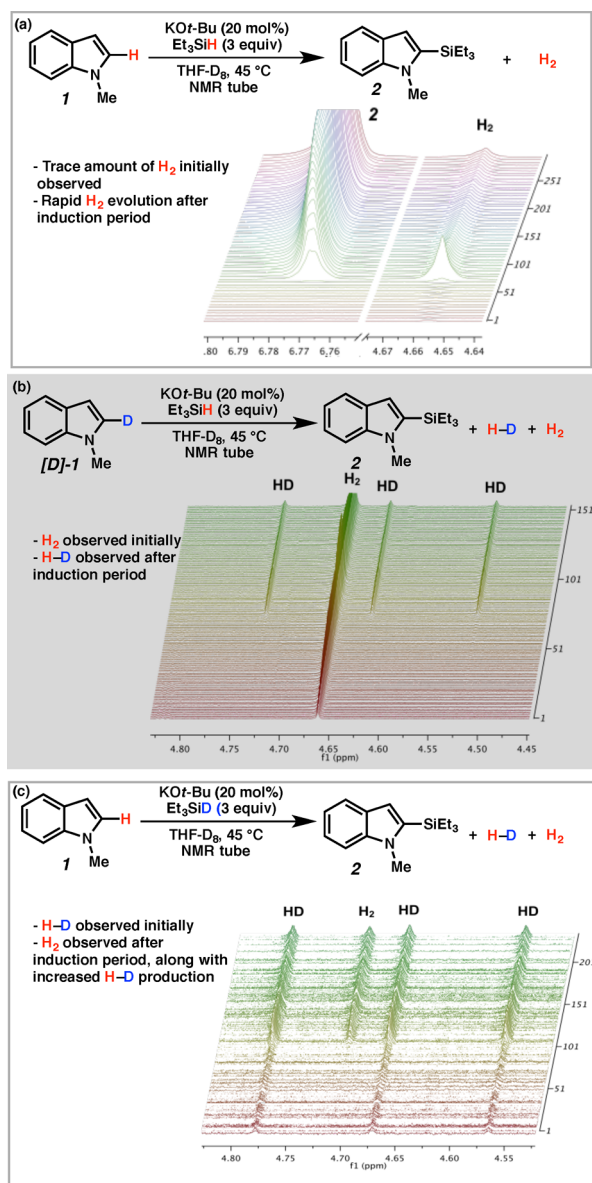


ment of **2** with both Et<sub>3</sub>SiH and *KOt*-Bu in THF led to the conversion of C2-silylated product **2** to C3-silylated product **3**, along with approximately 5% of desilylated product **1** (Scheme 2b). Moreover, a crossover experiment involving compound **2**, stoichiometric EtMe<sub>2</sub>SiH, and catalytic *KOt*-Bu provided a mixture of starting material **2**, cross-silylation product **4**, and desilylation product **1** (Scheme 2c). These results indicate that the conversion of C2- to C3-silylation product likely does not occur through intramolecular silyl migration. In fact, the observation of cross-silylation and desilylation can be better explained by a reversible silylation reaction under these conditions.

**Cross-Dehydrogenative Formation of H<sub>2</sub>.** The process of H<sub>2</sub> formation was probed by in situ NMR using deuterium-labeled substrates.<sup>20</sup> As shown in Scheme 3a, a trace amount of H<sub>2</sub> was detected during the induction period. This is followed by rapid H<sub>2</sub> evolution along with generation of the silylation product **2**. Similarly, H<sub>2</sub> is initially slowly generated in the case of the 2-deuterated indole [D]-**1**, Et<sub>3</sub>SiH, and *KOt*-Bu under identical conditions, followed by the cross-dehydrogenative formation of HD (1:1:1 triplet, *J* = 43 Hz) after the induction period (Scheme 3b). Further experimentation with indole **1** and Et<sub>3</sub>SiH was also conducted under the same conditions. Small amounts of HD were detected at the beginning of the NMR study and further HD gas formation was observed with the formation of product (Scheme 3c). These data demonstrate that H<sub>2</sub> is generated from the cross-dehydrogenative pathway; moreover, a very small percentage of H<sub>2</sub> may be produced from the consumption of trace amounts of water or the radical initiation process.<sup>21</sup> Furthermore, large-scale reactions were performed and gas evolution was monitored via eudiometry (Figure 3). The results from two identical runs produced H<sub>2</sub> in 69–71% yields, consistent with yields of silylation product **2** based on <sup>1</sup>H NMR and the plot of H<sub>2</sub> vs time correlates well to a plot of silylation product **2** vs time (Figure 3 vs Figure 1).

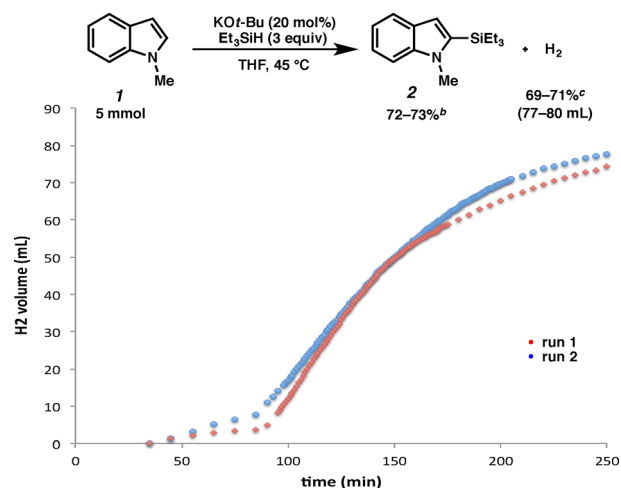
To probe the nature of the induction period, we performed a series of experiments using TEMPO as a radical inhibitor. As shown in Figure 4, although the addition of 3 mol% of TEMPO at the beginning of the reaction essentially doubles the delay in product formation (i.e., TEMPO inhibition plus induction) in contrast to the reaction without TEMPO (Figure 4, plot A), the conversions are comparable after 8 h (plot B). Similar trends were observed when TEMPO was added after the initiation period (i.e., at 3.33 h with 54% conversion, plots C and D); the product formation ceased for a period and then continued. A larger TEMPO addition, 6 mol% compared to 3 mol%,

## Scheme 3. Hydrogen Gas Formation through Dehydrogenative Coupling

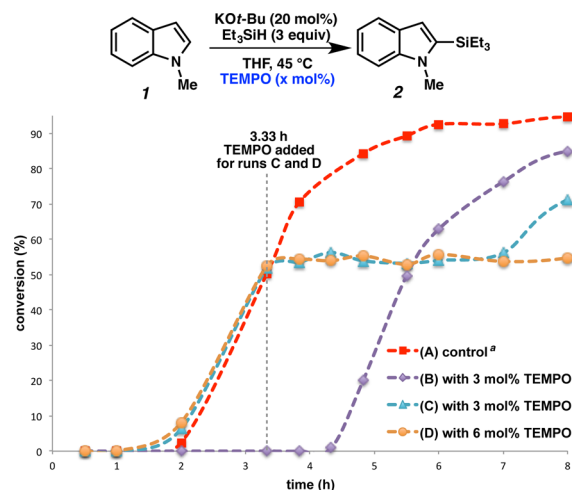


prolongs the resultant induction period accordingly. Interestingly, the addition of TEMPO to the initiated reaction mixture leads to immediate bleaching (from dark purple to light yellow), with the dark purple color returning over the period of hours. Careful analysis of the reaction with stoichiometric TEMPO by GC-MS displayed a signal with *m/z* that matches the expected mass of the TEMPO–SiEt<sub>3</sub> adduct formed from the capture of the triethylsilyl radical by TEMPO.<sup>22</sup> These experiments suggest that by coupling with the silyl radical, TEMPO terminates the radical chain process and the reaction restarts only after the substoichiometric amount of TEMPO has been fully consumed.<sup>23</sup> Further studies found that the mixture of KOt-Bu and Et<sub>3</sub>SiH in THF at 45 °C is EPR active.

Based on these results, we postulate that a silyl radical species is involved in this catalytic C–H silylation reaction. Our efforts were focused on the understanding of radical initiation under the standard reaction conditions. Although there are a considerable number of examples of silyl radical reactions known in the literature, the means of generating silyl radicals



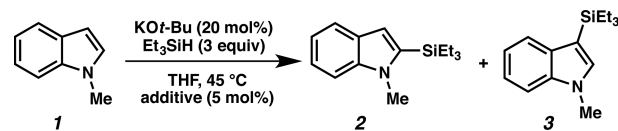
**Figure 3.** Hydrogen gas evolution. <sup>a</sup>Reaction conditions: 1 (5 mmol), Et<sub>3</sub>SiH (15 mmol), and KOt-Bu (1 mmol, 20 mol%) in THF (5 mL) (conducted in duplicate). <sup>b</sup>Conversion, determined by <sup>1</sup>H NMR. <sup>c</sup>Yield based on collected H<sub>2</sub> volume.



**Figure 4.** Reaction profiles with TEMPO addition. <sup>a</sup>Reaction conditions: 1 (0.5 mmol), Et<sub>3</sub>SiH (1.5 mmol), and KOt-Bu (0.1 mmol, 20 mol%) in THF (0.5 mL) at 45 °C. <sup>b</sup>With 3 mol% TEMPO added at the beginning of the reaction. <sup>c</sup>With 3 mol% of TEMPO added during the reaction at *t* = 3.33 h. <sup>d</sup>With 6 mol% of TEMPO added during the reaction at *t* = 3.33 h, product formation resumes at 11 h. Conversion was determined by monitoring aliquots via GC.

are rather limited.<sup>24</sup> In our case, the silylation reaction results in comparable yields when kept in the dark as exposed to ambient light, which rules out the possibility of visible light-induced radical formation. Recently, Itami, Lei and others reported that KOt-Bu could mediate the cross-coupling of aryl bromide and benzene without the use of transition-metal catalysis.<sup>25</sup> Subsequent mechanistic studies revealed that in the presence of 1,10-phenanthroline a radical species was generated.<sup>26</sup> This process is accelerated dramatically with catalytic amounts of organic electron transfer reagents, such as *N*-methylpyrrolidone, *N*-methylglycine, and glycine, as demonstrated by Murphy.<sup>27</sup> However, in our silylation reaction, the addition of any of these compounds resulted in a significant decrease in reactivity (Table 3, entries 1–4).

A reported method for the generation of silane based radicals is the abstraction of a hydrogen atom from hydrosilanes using

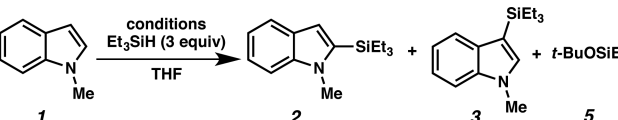
Table 3. Effect of Additives<sup>a</sup>


entry	additive	time (h)	conv (%) <sup>b</sup>	2:3 <sup>b</sup>
1	1,10-phenanthroline	8	52	>20:1
		24	79	>20:1
2	<i>N</i> -methylpyrrolidone	8	0	>20:1
		24	50	>20:1
3	<i>N</i> -methylglycine	8	7	>20:1
		24	67	19:1
4	glycine	8	10	>20:1
		24	54	>20:1
5	none	8	93	>20:1

<sup>a</sup>Reaction conditions: **1** (0.5 mmol), Et<sub>3</sub>SiH (1.5 mmol), KO*t*-Bu (0.1 mmol, 20 mol%), and additive (5 mol%) in THF (0.5 mL) at 45 °C.

<sup>b</sup>Determined by GC analyses.

organic radicals (e.g., *n*-Bu<sub>3</sub>Sn•, *t*-BuO•).<sup>28</sup> To test whether this mechanism is involved in our reaction, we have undertaken a series of experiments with *tert*-butoxyl radicals generated in situ. No product was obtained with 20 mol% of di-*tert*-butyl peroxide (DTBP) at 135 °C (Table 4, entry 2). Utilizing

Table 4. Effect of *tert*-Butoxy Radical Precursors<sup>a</sup>


entry	conditions	amount (mol%)	temp (°C)	time (h)	conv (%) <sup>b</sup>	detection of <b>5</b> <sup>b</sup>
1	KO <i>t</i> -Bu	20	45	24	80	yes
2	DTBP	20	135	14	1	no
3	DTBP	100	135	14	10	no
4	DTBP + KO <i>t</i> -Bu	20, 20	45	14	42	yes
5	TBHN	10	45	10	0	no
				24	0	no
6	TBHN + NaO <i>t</i> -Bu	10, 20	45	10	0	no
				24	0	no
7	TBHN + KO <i>t</i> -Bu	10, 20	45	10	0	no
				24	54	yes

<sup>a</sup>Reaction conditions: **1** (0.5 mmol), Et<sub>3</sub>SiH (1.5 mmol), KO*t*-Bu (0.1 mmol, 20 mol%, if used), and radical initiator in THF (0.5 mL) at 45 °C. <sup>b</sup>Determined by GC analyses.

stoichiometric DTBP at 135 °C led to only small amounts of desired product along with very complicated mixtures as indicated by the GC-MS traces (entry 3). Attempts to carry out the silylation reaction under milder conditions with 10 mol% of di-*tert*-butyl hyponitrite (TBHN) or a mixture of TBHN and NaO*t*-Bu failed to furnish product (entries 5 and 6). Addition of KO*t*-Bu with either DTBP or TBHN furnished the desired silylation product, albeit with decreased yields (entries 4 and 7). Moreover, under our standard reaction conditions (i.e., entry 1), the desired product was always accompanied by *t*-BuOSiEt<sub>3</sub> (**5**). The reactions with DTBP or TBHN did not produce *t*-BuOSiEt<sub>3</sub>, which suggests that *t*-BuOSiEt<sub>3</sub> may not be formed through the reaction of *t*-BuO• with hydrosilane or silyl radical, but through a differing pathway (vide infra). Although the

involvement of a *tert*-butoxy radical cannot be excluded on the basis of these experiments, there is little evidence to support the initiation of a triethylsilyl radical via hydrogen atom abstraction from Et<sub>3</sub>SiH by *tert*-butoxy radical.

**Investigation of Coordinated Silane Species by FTIR Studies.** It has been well documented that the addition of strong silicophilic Lewis bases (e.g., fluoride, alkoxide) can increase the reactivity of hydrosilanes in the hydrosilylation of C=O bonds.<sup>29</sup> It is believed that strongly reducing hypercoordinate silicate complexes are formed by coordination of nucleophilic anions during such processes, which typically weakens the Si–H bond and increases the hydridic character of this bond.<sup>30,31</sup> Studies by Corriu et al. revealed that the direct reaction of (RO)<sub>3</sub>SiH with the corresponding KOR (R = alkyl or aryl) in THF at room temperature affords the anionic, five-coordinate hydrosilicate [HSi(OR)<sub>4</sub>]K in good yield.<sup>32</sup> Such species are found to be very effective in the reduction of carbonyl compounds, can act as an electron donor toward the dehalogenation of organic halides, or can donate one electron to a metal complex.<sup>32</sup> Although the formation of similar pentacoordinate species from trialkylsilanes and potassium alkoxide is unknown, we envisioned that such a complex is a possible intermediate in our reaction and may play a crucial role in radical initiation.

Unfortunately, attempts to isolate and structurally characterize such species by NMR were unsuccessful.<sup>33</sup> However, by monitoring the silylation reaction using ReactIR, we found evidence for the existence of a new, possibly pentacoordinate silicate species. As shown in Figure 5, the in situ IR spectrum, a

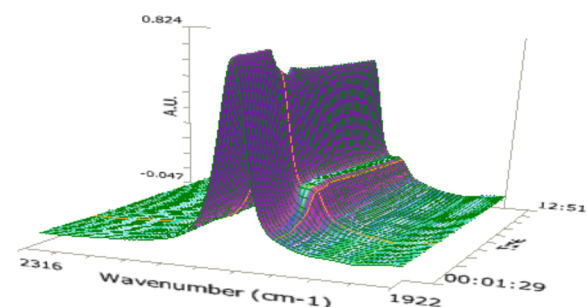


Figure 5. ReactIR plot of KO*t*-Bu and Et<sub>3</sub>SiH in THF. New peak adjacent to Si–H signal of Et<sub>3</sub>SiH clearly visible.

new peak is visible at 2056 cm<sup>-1</sup>, adjacent to the Si–H stretching band in Et<sub>3</sub>SiH (2100 cm<sup>-1</sup>). This lower frequency peak would be consistent with an elongated, weakened Si–H axial bond in a five-coordinate silicate, as expected in such pentacoordinate complexes.<sup>34</sup> A similar shift was reported previously by Mittel et al. for the *trans* Si–H stretching in *N,N*-dimethylaminopropylsilane ([H<sub>3</sub>Si(CH<sub>2</sub>)<sub>3</sub>NMe<sub>2</sub>]) from 2151 to 2107 cm<sup>-1</sup>.<sup>35</sup> In this case, the authors rationalize that the observed redshift occurs by an N–Si interaction to form a hypercoordinate complex, as confirmed by X-ray analysis.

A correlation between the newly formed IR peak (Figure 5) and the onset of product formation (i.e., the induction period ending) was observed. Once the new IR peak reached a steady state, the consumption of indole **1** and formation of silylation product **2** occur immediately. Furthermore, the new IR peak was visible throughout the reaction. This is consistent with the observation that premixing Et<sub>3</sub>SiH and KO*t*-Bu in THF for 2 h at 45 °C followed by the addition of indole **1** eliminates the induction period, suggesting that the formation of penta-

coordinate silicate is responsible for the observed induction period.

Further studies were undertaken with mixtures of  $\text{Et}_3\text{SiH}$  and metal alkoxides listed in Table 1, utilizing ATR-FTIR in a nitrogen-filled glovebox after removal of the volatiles (i.e., THF,  $\text{Et}_3\text{SiH}$ ). As shown in Figure 6, any alkoxide base which was a

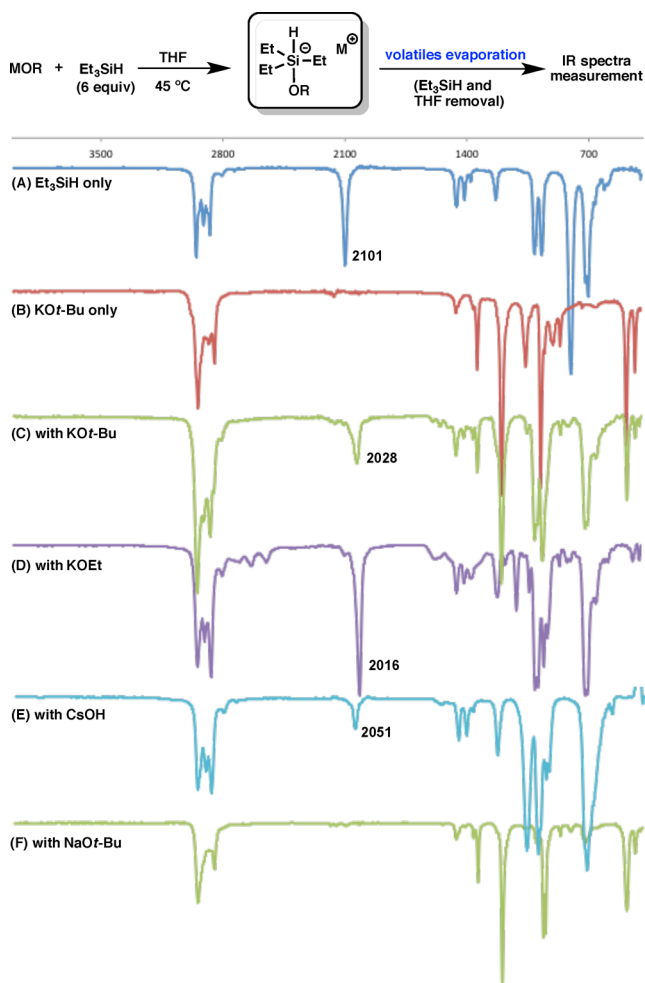


**Figure 6.** FTIR spectra of Si–H stretching region of select metal alkoxides with hydrosilane. Spectra were acquired under an atmosphere of  $\text{N}_2$  and are normalized and stacked for clarity; see SI for full spectra: (A) neat  $\text{Et}_3\text{SiH}$ ; (B) neat  $\text{KOt-Bu}$ ; (C–F) prepared as indicated with  $\text{MOR} = \text{KOt-Bu}$ ,  $\text{KOEt}$ ,  $\text{CsOH}$ , and  $\text{NaOt-Bu}$ , respectively.

competent silylation catalyst developed a lower energy Si–H feature (from 2016–2051  $\text{cm}^{-1}$ , see SI for details), potentially corresponding to the Si–H bond of a pentacoordinate species. In sharp contrast, no such species were detected with unreactive catalysts [i.e.,  $\text{LiOt-Bu}$ ,  $\text{NaOt-Bu}$  (Figure 6F), alkali earth metals, or aluminum alkoxides], demonstrating that this new pentacoordinate complex is likely crucial for the radical initiation. For the pentacoordinate silicates formed from  $\text{KOt-Bu}$  and  $\text{KOEt}$ , the decrease in the frequencies of Si–H absorption correlates to a shortening of the induction period, which is consistent with a longer bond requiring less energy for the homolytic cleavage (Figure 6c and 6d).

Finally, although there is a large variation in the induction periods with  $\text{KOH}$ ,  $\text{RbOH}$ , and  $\text{CsOH}$ , no differentiating Si–H frequencies of the pentacoordinate silicates derived from those

bases are observed.<sup>36</sup> It is possible that the weak cation–anion interaction of late alkali metal bases could accelerate the formation of pentacoordinate silicates and thus account for the differing rate of radical initiation.<sup>37</sup>

We also performed computational studies to understand the nature of the coordinated species. Figure 7 shows the calculated

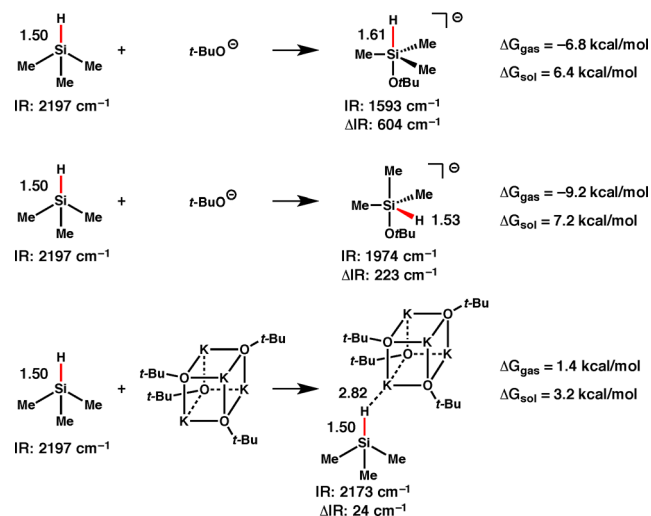


**Figure 7.** Calculated energetics of formation of pentacoordinate silicates or tetrameric  $\text{KOt-Bu}$  associated silane complex and the calculated IR stretching frequency of the Si–H bond. The Si–H bond lengths are given in angstroms.

energetics of complex formation and the predicted Si–H stretching frequencies. Formation of the pentacoordinate silicate with the hydrogen atom in the axial position requires 6.4 kcal/mol, and with hydrogen in the equatorial position requires 7.2 kcal/mol. In both cases the pentacoordinate species are stable minima; however, the entropy penalty of 12 kcal/mol for a 1 M standard state causes the corresponding free energies to be unfavorable. The predicted IR shifts from trimethylsilane to these two silicate isomers are 604 and 223  $\text{cm}^{-1}$ , respectively. Both of these IR shifts are larger than the experimentally observed IR shift of 73  $\text{cm}^{-1}$ . The formation of tetrameric  $\text{KOt-Bu}$  associated silane complex is 3.2 kcal/mol endergonic, and the IR shift from silane to the corresponding  $(\text{KOt-Bu})_4$  associated silane complex is only 24  $\text{cm}^{-1}$ . The M062x functional and various basis sets were tested to probe the energetics of formation of these coordinated silicon species and provided similar results (see SI, Figure S1).

**Radical Initiation.** The bond dissociation energy for the Si–H bond of  $\text{Et}_3\text{SiH}$  is 90.1 kcal/mol,<sup>38</sup> and the corresponding Si–H bond of silicate 6 would be weakened due to a change in electronics in the pentacoordinate structure.<sup>34</sup> Thus, a possible pathway for the radical initiation from silicate 6 would be the homolytic scission of Si–H to form a hydrogen radical (likely associated with other substances, e.g., solvent, substrate, or base) and a coordination anion-radical complex 7 (consistent with the resultant  $t\text{-BuOSiEt}_3$  detected by GC after workup of the reaction), as shown in Figure 8a. This hydrogen radical could then abstract a hydrogen atom from  $\text{Et}_3\text{SiH}$  to generate hydrogen gas, as detected by in situ  $^1\text{H}$  NMR, and a triethylsilyl radical, which we believe is the active species.<sup>39</sup>

Unfortunately, our attempts to calculate such a radical initiation mechanism resulted in large activation energies

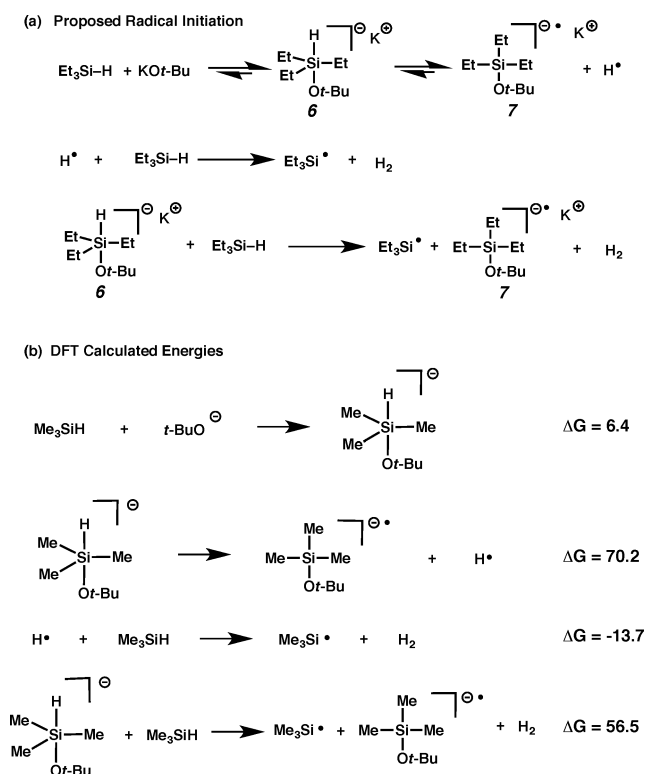


**Figure 8.** (a) Possible radical initiation: homolytic Si–H bond fission of hypercoordinate silane 6. (b) DFT-calculated energetics of the generation of silyl radical through homolytic Si–H bond fission of hypercoordinate silicate.<sup>40</sup> Gibbs free energies including THF solvation are shown in kcal/mol.

(Figure 8b). While we still believe a Si–H bond homolysis of a pentacoordinate silicate may be relevant given our aforementioned observations, we turned to DFT calculations to explore alternative initiation mechanisms with more reasonable activation energies.

#### Catalyst Speciation and Alternate Initiation Pathway.

The extent of KO $t$ -Bu aggregation in this reaction may be key to determining its catalytic behavior. The X-ray structure of anhydrous KO $t$ -Bu crystallized from THF– $n$ -pentane reveals a tetrameric [KO $t$ -Bu]<sub>4</sub>, with a cubane-like structure.<sup>41</sup> This tetrameric structure is very stable and persists in the solid and gas phase. Even in solution, mild Lewis basic solvents such as THF and diethyl ether do not break up the tetramer, and the calculated energy of dissociation shows that these processes are very unfavorable (Figure 9). Indeed, even the dissociation of tetramer (KO $t$ -Bu)<sub>4</sub> to trimer (KO $t$ -Bu)<sub>3</sub> associated with K<sup>+</sup> plus  $t$ -BuO<sup>−</sup> anion requires 25.9 kcal/mol. Therefore, the tetramer [KO $t$ -Bu]<sub>4</sub> is used as reference point in further calculations unless otherwise noted.

Our computational results show that the radical initiation pathway through homolytic Si–H bond fission of hypercoordinate silane is relatively high in energy (Figure 8). To address this unrealistic barrier, we have explored many different pathways of generation of the silyl radical (see SI, Figure S2), the most reasonable of which is shown in Figure 10.

We postulate that trace molecular oxygen might serve as a temporary electron acceptor to drive the formation of  $t$ -butoxide radical.<sup>42</sup> Upon reaction of dioxygen with tetramer [KO $t$ -Bu]<sub>4</sub>,  $t$ -butoxyl radical and potassium peroxide radical C-3 are generated. This process requires 23.4 kcal/mol, while

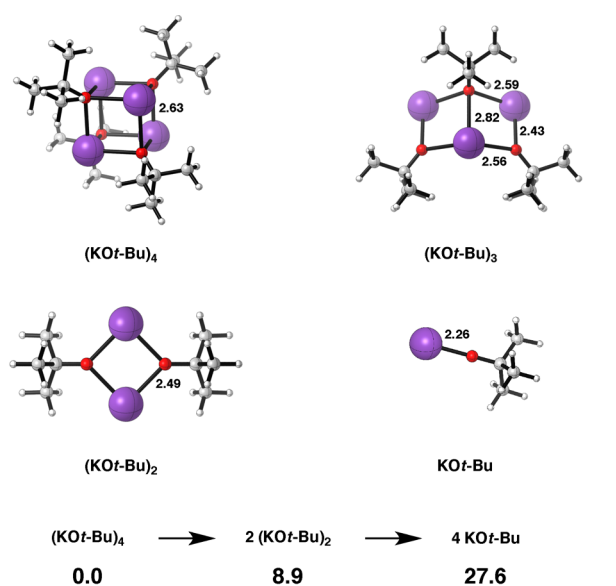


**Figure 9.** Dissociation of potassium  $t$ -butoxide to tetramer, trimer, dimer, and monomer in THF. Gibbs free energies are shown in kcal/mol. Bond distances are shown in angstroms.

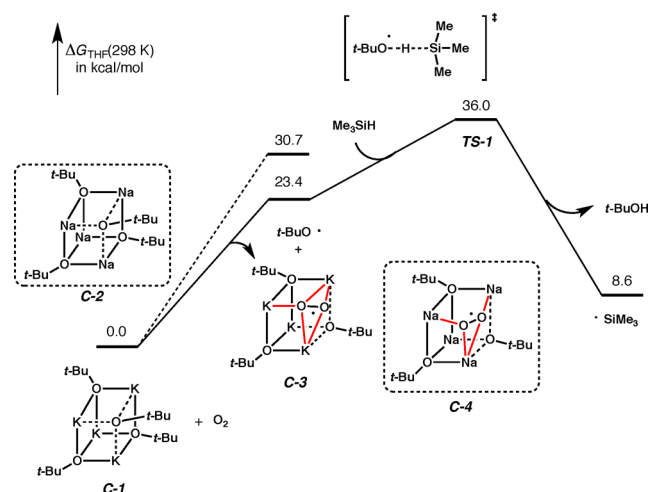


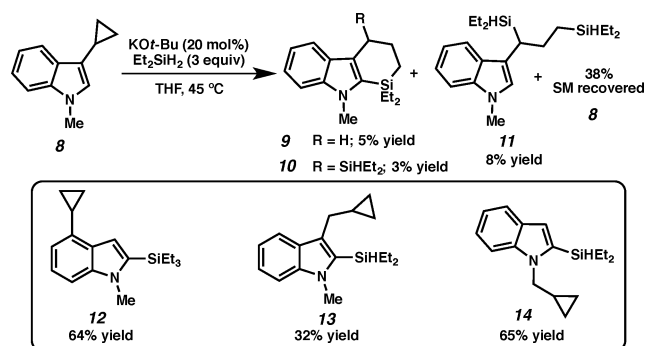
**Figure 10.** Free energy profile for generation of silyl radical involving traces of oxygen. Gibbs free energies, including THF solvation, are shown in kcal/mol.

the same process with tetramer [NaO $t$ -Bu]<sub>4</sub> requires 30.7 kcal/mol, shown as a dashed line in Figure 10. This is consistent with the failure of NaO $t$ -Bu as a catalyst for the silylation reaction. This effect can be understood since the smaller sodium ion size would lead to a larger distortion from the tetramer structure C-2 to sodium peroxide radical C-4, as compared to two K–O bonds formed when KO $t$ -Bu is used. Once the  $t$ -butoxyl radical is formed, it can react with hydrosilane Me<sub>3</sub>SiH to generate the silyl radical through transition state TS-1 (36.0 kcal/mol, Figure 10). This whole silyl radical generation process is endergonic by 8.6 kcal/mol.

mol, but only a trace amount of radicals is needed to initiate the proposed chain mechanism. This high-energy barrier for initiation would be consistent with the observed induction period. An alternative radical initiation mechanism is presented in the accompanying paper on ionic and neutral mechanisms.<sup>11</sup> This mechanism closely resembles that in Figure 10, but produces a hydroxyl radical instead of a *tert*-butoxyl radical and has a lower overall energy barrier of 24.7 kcal/mol.

**Radical Clock Experiments and Kinetic Isotopic Effects (KIEs).** To better understand how the triethylsilyl radical reacts with indole, cyclopropane-containing substrates were employed as radical probes in an attempt to trap radical intermediates. Several indole substrates bearing cyclopropyl or cyclopropylmethyl groups were synthesized and subjected to the silylation reaction conditions. With 3-cyclopropyl-substituted indole **8**, a mixture of ring-opened products were observed, including both silyl radical C2 adducts **9** and **10**, and hydrogen radical C2 adduct **11** (Scheme 4). The low yields of

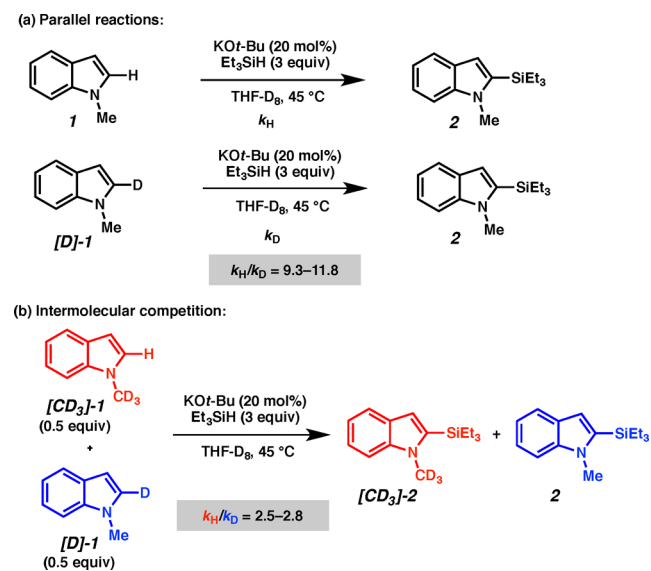
**Scheme 4. Silylation Using Cyclopropyl-Containing Substrates**



these trapped products may be explained by the termination of radical chain process by ring-opening and subsequent radical recombinations (see SI for details). In comparison, substrates with 4-cyclopropyl, 3-cyclopropylmethyl, and 1-cyclopropylmethyl substitution delivered the desired silylation products **12**, **13**, and **14**, respectively, in moderate yields without the detection of ring-opening reactions. These experiments support our hypothesized pathway which involves a C3-centered radical intermediate **15** (Scheme 6).

We envisioned that a  $\beta$  C–H fission from a C3-centered radical species (**15**, see Scheme 6) resulting in the formation of hydrogen gas is most likely the rate-determining step of the proposed radical chain process. To gather more information about this hypothesis, C2-deuterium-labeled indole ([D]-1) was used to study the KIEs during the C2-silylation. First, two separate, parallel reactions of triethylsilane with indoles **1** and [D]-1 were performed to determine the KIE value (Scheme 5a). As monitored by in situ <sup>1</sup>H NMR, a significant KIE was observed using the initial rates method for each reaction at the onset of product formation ( $k_H/k_D = 9.3$ – $11.8$ , see SI for details). The intermolecular competition reaction of [D]-1 and 1-CD<sub>3</sub>-indole [CD<sub>3</sub>]-1 in the same pot also showed a clear isotopic effect ( $k_H/k_D = 2.5$ – $2.8$ , see SI for details) calculated from the product ratio of [CD<sub>3</sub>]-2 and **2**. These results provide evidence that the C–H bond breaking of indole is involved in the rate-determining step. We also investigated the reaction using Et<sub>3</sub>SiH and Et<sub>3</sub>SiD, finding that the reactions with deuterated silane demonstrated a significantly longer induction

**Scheme 5. Isotope Effect of Deuterium-Labeled Substrates**



period, and a decreased reaction rate was observed (see SI for details). We rationalized these differences since the homolytic cleavage of a Si–D bond in a pentacoordinate species would require higher energy, prolonging the induction period. Furthermore, the slower abstraction of deuterium compared to hydrogen limits the overall reaction rate in the radical chain mechanism.<sup>43</sup>

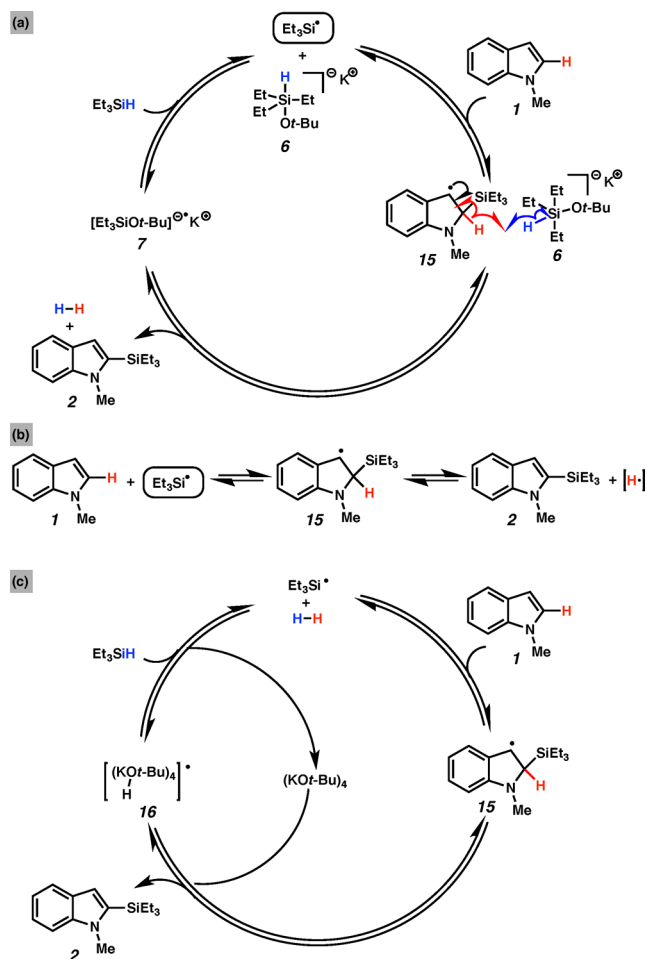
**Proposed Cycle.** The addition of silyl radicals to double bonds has been shown to readily occur, driven by the formation of a stronger  $\sigma$ -bond at the expense of a weaker  $\pi$ -bond.<sup>44</sup> Therefore, we propose that Et<sub>3</sub>Si• adds to indole at the C2 position to generate a stabilized benzylic radical **15** (Scheme 6a), as evidenced by radical clock experiments shown in Scheme 4. Fragmentation of the weaker C2–H bond  $\alpha$  to the radical center by a  $\beta$ -H scission restores aromaticity in the indole system and generates H<sub>2</sub>, providing an entropic driving force for the overall reaction.<sup>45,46</sup> The resultant silicate radical anion **7** can then react with an equivalent of triethylsilane, thereby regenerating Et<sub>3</sub>Si•, continuing the chain process. Alternatively, tetrameric (KOt-Bu)<sub>4</sub> could act as a hydrogen atom transfer catalyst, by abstracting a hydrogen atom from benzylic radical **15**, producing the silylated product **2** as well as the base-hydrogen radical adduct **16** (Scheme 6c). This radical adduct then reacts with another equivalent of hydrosilane to produce H<sub>2</sub> and regenerates the silyl radical, thus completing the catalytic cycle.

The significant KIE displayed by [D]-1 suggests that the  $\beta$ -H scission is the rate-determining step after radical initiation. The nucleophilic  $\beta$ -silyl radical **15** is slow to abstract a hydrogen atom from Et<sub>3</sub>Si–H due to the similar polarities of the two radicals (i.e., **15** vs Et<sub>3</sub>Si•), and a hydrosilylation product was never observed.<sup>47</sup> The reversibility of the silylation reaction can be explained by the addition of H• to silylation product **2**, providing radical **15**, followed by C–Si bond scission to form an equivalent of Et<sub>3</sub>Si• instead of H•, resulting in the formation of starting material (Scheme 6b, reverse).

**Reaction with Deuterium-Labeled Silolane as a Stereochemical Probe.** To gain further evidence for the proposed reaction mechanism, we envisioned using a method to study the stereochemical course at silicon during the C–H silylation. Since the synthesis of silicon-stereogenic silanes



**Scheme 6. Proposed Chain Process: Radical Pathway Mediated by Pentacoordinate Silicon (a) or Tetrameric KOt-Bu (c)**



(chiral silane) and determination of stereochemical outcomes in Si–C bond-forming reactions (i.e., determination of the absolute configuration of the silylated product) are challenging,<sup>48</sup> we decided to utilize a method recently reported by the Oestreich group. In this method, a mixture of isomers of deuterium-labeled silolanes **17** are used as a stereochemical probe (Figure 11).<sup>49</sup> The *syn* and *anti* designations are the relative orientation of deuterium to the *n*-hexyl group.

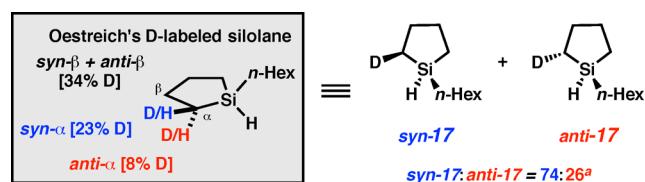


**Figure 11.** Oestreich's deuterium-labeled silolane. <sup>a</sup>*Syn:anti* ratio determined by <sup>2</sup>H NMR. <sup>b</sup>Deuteration at the β position is omitted for clarity.

<sup>2</sup>H NMR allows for tracking the relative ratio of *syn-17* and *anti-17* and therefore determining configurational changes at the silicon atom on the basis of changes in the *syn:anti* ratio, thus removing the need to know the exact distribution of deuterium in this complex mixture of isomers.

Oestreich's deuterium-labeled silolane was prepared according to the reported procedure, resulting in a mixture of isomers with a *syn-17/anti-17* ratio of 74:26. Interestingly, KOt-Bu-catalyzed silylation of **18** under our previously reported conditions proceeds with complete scrambling of the configuration at the silicon atom, as indicated by the 1:1 ratio of products *syn-19* and *anti-19* (Figure 12).

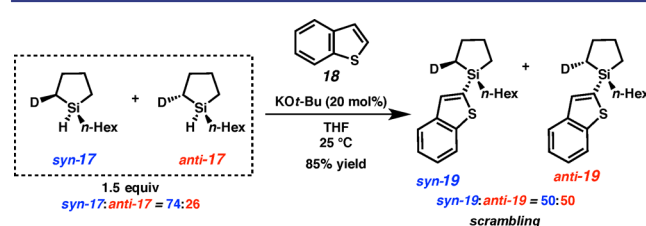


**Figure 12.** Following the stereochemistry of C–H silylation: scrambling of the configuration at the silicon atom.

This observed scrambling is in contrast to Falck's protocol using an iridium(I) catalyst, where complete retention of the stereochemistry at the silicon atom is observed due to a traditional oxidative addition/reductive elimination pathway.<sup>49,50</sup> Previous studies by Sommer, Oestreich, and others have shown that a nucleophilic substitution at the silicon center can occur with either retention or inversion of stereochemistry, depending on the nature of the nucleophile and the leaving group on silicon.<sup>51</sup> Yet these reactions are highly stereospecific and do not result in scrambling of the deuterium-labeled silolane.<sup>49</sup>

We theorized that the observed scrambling may occur without participation of the heteroarene. A control experiment treating a mixture of **17** with KOt-Bu alone in THF resulted in complete scrambling of the deuterium-labeled silolane (Figure 13).

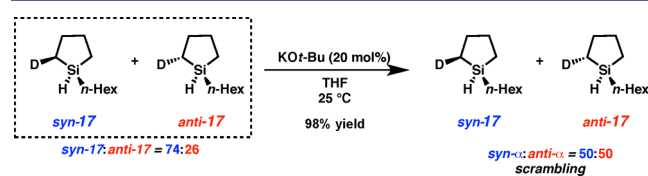


**Figure 13.** Base-catalyzed scrambling of the configuration at silicon.

While stereochemical scrambling is consistent with a number of our proposed intermediates, we cannot distinguish if it occurs at the stage of pentacoordinate silicate anion **6**, radical anion **7**, or a tricoordinate silyl radical (cf. Figure 8). Pentacoordinate silicon intermediates may undergo pseudo-rotational processes resulting in loss of stereochemical information at the silicon atom.<sup>52</sup> Although silyl radicals are pyramidal and can be configurationally stable under certain conditions,<sup>53</sup> racemization of a chiral silyl radical could take place due to the fast inversion of the pyramidal radical.<sup>54</sup> Nevertheless, all three of these intermediates are on the pathway in our proposed mechanism (Scheme 6).

Furthermore, a handful of examples of direct nucleophile trapping by a hydrosilane are known in the literature, including KOt-Bu-catalyzed protection of alcohols.<sup>55</sup> In this case, retention at the silicon center was observed with a chiral silane,<sup>55b</sup> which is not in line with our observed scrambling.

**Computational Study of the C–H Silylation Mechanism and Regioselectivity.** We have performed a computational study that explores the mechanism and origin of regioselectivity of this C–H silylation reaction. We propose that the reaction can proceed by either of the two radical chain mechanisms shown in Scheme 6. The free energies of both C2- and C3-silylation of 1-methylindole are shown in Figures 14 and 15, for the cycles in Scheme 6a and 6c, respectively.

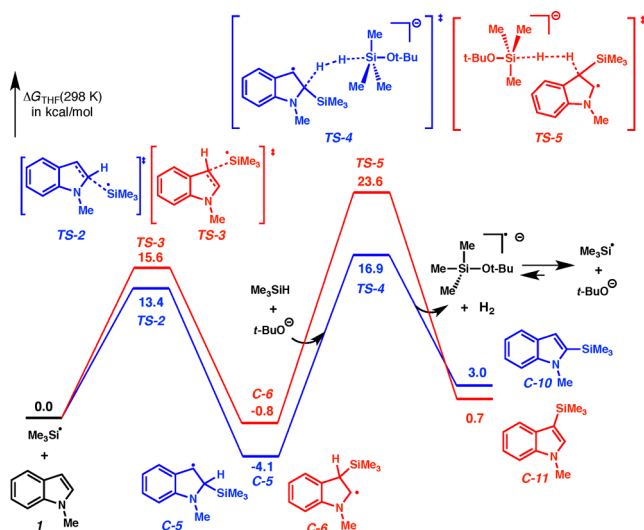


**Figure 14.** Free energy profile for C–H silylation of 1-methylindole at C2 and C3 positions. Hydrogen atom is abstracted by pentacoordinate silicate anion. Gibbs free energies including THF solvation are shown in kcal/mol.

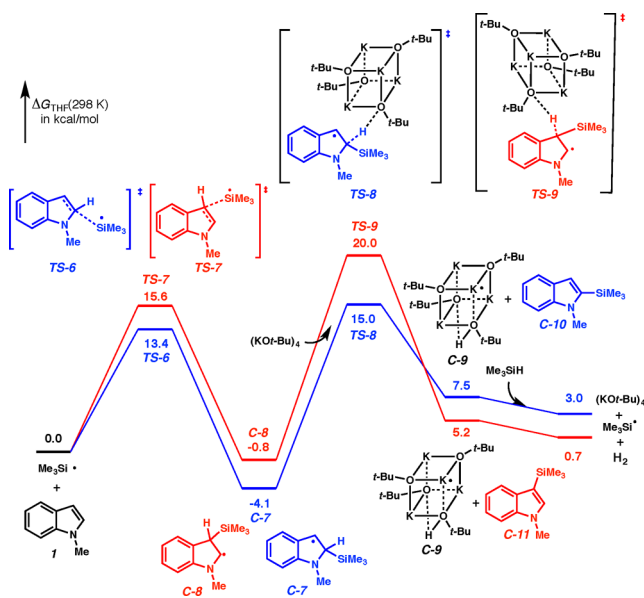


**Figure 15.** Free energy profile for C–H silylation of 1 at the C2 and C3 positions. Hydrogen atom is abstracted by tetrameric (KOt-Bu)<sub>4</sub>. Gibbs free energies, including THF solvation, are shown in kcal/mol.

Starting with the trimethylsilyl radical, the radical addition is facile and reversible, generating intermediate C-5. The pentacoordinate silicate anion can then abstract the ipso hydrogen atom to generate H<sub>2</sub> gas, silylation product, and silicate radical anion. The silicate radical anion then dissociates to form silyl radical and *tert*-butoxide anion. Hydrogen atom

abstraction is the rate-determining step, with a calculated barrier of 21.0 kcal/mol for C2-silylation.

Since the radical addition to 1-methylindole is fast and reversible, the subsequent hydrogen abstraction determines the regioselectivity. The hydrogen abstraction at the C2 position, via TS-4, is lower than the competing hydrogen abstraction at the C3 position, via TS-5, by 6.7 kcal/mol.

Alternatively, the mechanism in which (KOt-Bu)<sub>4</sub> acts as a hydrogen atom transfer catalyst is shown in Figure 15. The hydrogen atom abstraction at the C2 position, via TS-8, requires 19.1 kcal/mol. This pathway is lower in energy than TS-4, which requires 21.0 kcal/mol with *t*-BuO<sup>−</sup> or 46.9 kcal/mol based on (KOt-Bu)<sub>4</sub>. Therefore, computational models predict that the hydrogen atom abstraction by tetrameric (KOt-Bu)<sub>4</sub> is favorable compared to direct hydrogen evolution by pentacoordinate silicate anion.

TS-8 and TS-4 are lower in energy than TS-9 and TS-5 for the competing hydrogen abstraction at the C3 position, indicating that the C2 silylation product is the kinetic product. This result is consistent with the experimentally observed C2-silylation regioselectivity at room temperature (cf. Table 2). At higher temperatures or longer reaction times, C3-silylation becomes the major product. The calculations indicate that the C3-silylation product is 2.3 kcal/mol lower in energy than the C2-silylation product. This is consistent with the experimental observation that C3-silylation is the thermodynamic product.

We also studied the reactivities of various five-membered heterocycles (1-methylpyrrole, furan, and thiophene). The relative rates from competition experiments are thiophene > furan > 1-methylpyrrole.<sup>10</sup> Our computational results show that 1-methylpyrrole has the highest reaction barrier for C–H silylation at the C2 position in the 5-membered aromatic heterocycles (Figure 16). While electrophilic aromatic substitution reactions favor C3 regioselectivity, silyl radical additions favor C2 regioselectivity. This is due to the nucleophilic character of silyl radicals. The silyl radical is strongly bent out of the plane and highly prefers a pyramidal

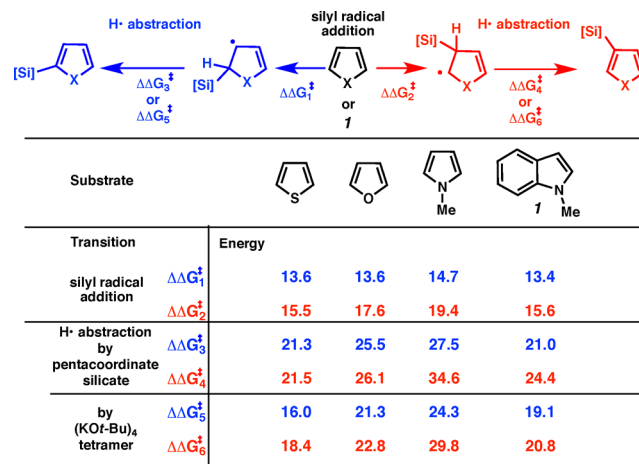


**Figure 16.** Calculated silyl radical addition barriers at C2 and C3 positions ( $\Delta\Delta G_1^\ddagger$  and  $\Delta\Delta G_2^\ddagger$ ), hydrogen abstraction barriers by pentacoordinate silicate anion at C2 and C3 positions ( $\Delta\Delta G_3^\ddagger$  and  $\Delta\Delta G_4^\ddagger$ ), and hydrogen abstraction barriers by tetrameric (KOt-Bu)<sub>4</sub> at C2 and C3 positions ( $\Delta\Delta G_5^\ddagger$  and  $\Delta\Delta G_6^\ddagger$ ) for C–H silylation of substrates 1-methylindole, 1-methylpyrrole, furan, and thiophene at C2 and C3 positions. Gibbs free energies including THF solvation are shown in kcal/mol.

structure. The singly occupied molecular orbital (SOMO) of silyl radical has a high percentage of 3s character,<sup>44</sup> and is more nucleophilic than electrophilic.

As seen in Figure 16, the product-determining step for each of the 5-membered aromatic heterocycles is lower for the C2 pathway (blue,  $\Delta\Delta G_3^\ddagger$  or  $\Delta\Delta G_5^\ddagger$ ) as compared to C3-silylation (red,  $\Delta\Delta G_4^\ddagger$  or  $\Delta\Delta G_6^\ddagger$ ), which matches with the observed experimental regioselectivity (i.e., C2 > C3).<sup>10</sup> Comparing the highest energy step for each of the 5-membered heterocycles highlights the expected inverse relationship of energy barrier to relative reaction rate (i.e., thiophene has the lowest energy barrier and demonstrates the highest rate in the competition reaction).

## CONCLUSIONS

We have reported a systematic mechanistic investigation of the KO<sup>t</sup>-Bu-catalyzed silylation of indoles. Specifically, a wide array of experimental tools, including NMR and ReactIR in situ studies, radical trap and radical clock experiments, and stereochemical analysis, etc., were applied to elucidate the pathway for the silylation reaction. These experimental results were further complemented by computational analysis of the reaction. The results of these experiments are consistent with a radical chain mechanism, wherein the triethylsilyl radical is generated by the thermal cleavage of Si–H bond of the coordinated silicon species or by traces of oxygen which facilitate radical formation. The radical clock and KIE experiments support a cycle in which C–Si bond formation through silyl radical addition and subsequent  $\beta$ -H scission regenerates the silyl radical and continues the chain process. Furthermore, the opening of only the cyclopropane near the C3 position of indole provides direct evidence for an indole radical intermediate. The overall reaction is reversible, with an equilibrium shifted toward product by the cross-dehydrogenative H<sub>2</sub> evolution as an entropic driving force. The use of deuterium-labeled silolane as a stereochemical probe supports a number of on-pathway intermediates in our postulated radical mechanism. Further studies will explore the relevance of such novel silyl radical mechanisms to other types of silylation or hydrosilylation reactions.

## ASSOCIATED CONTENT

### Supporting Information

The Supporting Information is available free of charge on the ACS Publications website at DOI: 10.1021/jacs.6b13031.

Full experimental procedures, FTIR spectra, characterization data, and Cartesian coordinates of computational structures (PDF)

## AUTHOR INFORMATION

### Corresponding Authors

\*houk@chem.ucla.edu

\*stoltz@caltech.edu

### ORCID

Yun-Fang Yang: 0000-0002-6287-1640

Hendrik F. T. Klare: 0000-0003-3748-6609

Martin Oestreich: 0000-0002-1487-9218

Donna G. Blackmond: 0000-0001-9829-8375

Richard N. Zare: 0000-0001-5266-4253

Robert H. Grubbs: 0000-0002-0057-7817

K. N. Houk: 0000-0002-8387-5261

Brian M. Stoltz: 0000-0001-9837-1528

### Author Contributions

#W.-B.L., D.P.S., and Y.-F.Y. contributed equally.

### Notes

The authors declare no competing financial interest.

## ACKNOWLEDGMENTS

The authors wish to thank the NSF under the CCI Center for Selective C–H Functionalization (CCHF) (CHE-1205646), CHE-1212767 for support, the Novartis Institutes for Biomedical Research Incorporated for the donation of samples to the CCHF, and CHE-1361104. Calculations were performed on the Hoffman2 cluster at UCLA and the Extreme Science and Engineering Discovery Environment (XSEDE), which is supported by the NSF. The Shanghai Institute of Organic Chemistry (SIOC) and S.-L. You are thanked for a postdoctoral fellowship to W.-B.L. D.P.S. thanks the CCI Center for Selective C–H Functionalization for support and the Blackmond group (TSRI) for their assistance and hospitality. A.A.T. is grateful to Bristol-Myers Squibb, the Resnick Sustainability Institute at Caltech, and Dow Chemical for predoctoral fellowship as well as to NSERC for a PGSD fellowship. M.O. is indebted to the Einstein Foundation (Berlin) for an endowed professorship. N.N. thanks Florida Tech for sabbatical leave and thanks B.M.S. and Caltech for hosting him in their research laboratories. We thank J. Buss (Caltech), N. Thompson (Caltech), Prof. Krenske (University of Queensland), and Prof. Jenkins (Griffith Univ.) for helpful discussions. The Peters, Bercaw, and Agapie groups (Caltech) are thanked for instrumentation. We thank Dr. Angelo Di Bilio for assistance in recording EPR spectra, Dr. Dave VanderVelde for NMR expertise, and Dr. Mona Shahgholi and Dr. Naseem Torian for mass spectrometry assistance (Caltech). We thank Claude Y. Legault for CYLView, used for the molecular graphics.<sup>56</sup>

## REFERENCES

- (1) (a) Liu, C.; Yuan, J.; Gao, M.; Tang, S.; Li, W.; Shi, R.; Lei, A. *Chem. Rev.* **2015**, *115*, 12138–12204. (b) DiRocco, D. A.; Dykstra, K.; Krska, S.; Vachal, P.; Conway, D. V.; Tudge, M. *Angew. Chem., Int. Ed.* **2014**, *53*, 4802–4806. (c) Bandini, M.; Eichholzer, A. *Angew. Chem., Int. Ed.* **2009**, *48*, 9608–9644. (d) Bergman, R. G. *Nature* **2007**, *446*, 391–393. (e) Godula, K.; Sames, D. *Science* **2006**, *312*, 67–72. (f) Labinger, J. A.; Bercaw, J. E. *Nature* **2002**, *417*, 507–514.
- (2) (a) Cernak, T.; Dykstra, K. D.; Tyagarajan, S.; Vachal, P.; Krska, S. W. *Chem. Soc. Rev.* **2016**, *45*, 546–576. (b) Jin, J.; MacMillan, D. W. C. *Nature* **2015**, *525*, 87–90. (c) Légaré, M.-A.; Courtemanche, M.-A.; Rochette, É.; Fontaine, F.-G. *Science* **2015**, *349*, 513–516. (d) Rossi, R.; Bellina, F.; Lessi, M.; Manzini, C. *Adv. Synth. Catal.* **2014**, *356*, 17–117. (e) O'Brien, A. G.; Maruyama, A.; Inokuma, Y.; Fujita, M.; Baran, P. S.; Blackmond, D. G. *Angew. Chem., Int. Ed.* **2014**, *53*, 11868–11871. (f) Fujiwara, Y.; Dixon, J. A.; O'Hara, F.; Funder, E. D.; Dixon, D. D.; Rodriguez, R. A.; Baxter, R. D.; Herlé, B.; Sach, N.; Collins, M. R.; Ishihara, Y.; Baran, P. S. *Nature* **2012**, *492*, 95–99.
- (3) (a) Ball, L. T.; Lloyd-Jones, G. C.; Russell, C. A. *Science* **2012**, *337*, 1644–1648. (b) Sore, H. F.; Galloway, W. R. J. D.; Spring, D. R. *Chem. Soc. Rev.* **2012**, *41*, 1845–1866. (c) Nakao, Y.; Hiyama, T. *Chem. Soc. Rev.* **2011**, *40*, 4893–4901. (d) Denmark, S. E.; Baird, J. D. *Chem. - Eur. J.* **2006**, *12*, 4954–4963. (e) Denmark, S. E.; Ober, M. H. *Aldrichimica Acta* **2003**, *36*, 75–85. (f) Langkopf, E.; Schinzer, D. *Chem. Rev.* **1995**, *95*, 1375–1408.
- (4) (a) Franz, A. K.; Wilson, S. O. *J. Med. Chem.* **2013**, *56*, 388–405. (b) Zhang, F.; Wu, D.; Xu, Y.; Feng, X. *J. Mater. Chem.* **2011**, *21*, 17590–17600. (c) Wang, Y.; Watson, M. D. *J. Am. Chem. Soc.* **2006**, *128*, 2536–2537. (d) Showell, G. A.; Mills, J. S. *Drug Discovery Today* **2003**, *8*, 551–556.

- (5) Hartwig, J. F. *Acc. Chem. Res.* **2012**, *45*, 864–873.
- (6) For reviews of catalytic C–H silylation, see: (a) Cheng, C.; Hartwig, J. F. *Chem. Rev.* **2015**, *115*, 8946–8975. (b) Yang, Y.; Wang, C. *Sci. China: Chem.* **2015**, *58*, 1266–1279. (c) Sharma, R.; Kumar, R.; Kumar, I.; Singh, B.; Sharma, U. *Synthesis* **2015**, *47*, 2347–2366. (d) Xu, Z.; Huang, W.-S.; Zhang, J.; Xu, L.-W. *Synthesis* **2015**, *47*, 3645–3668.
- (7) Whisler, M. C.; MacNeil, S.; Snieckus, V.; Beak, P. *Angew. Chem., Int. Ed.* **2004**, *43*, 2206–2225. Also see ref 3f.
- (8) (a) Cheng, C.; Hartwig, J. F. *J. Am. Chem. Soc.* **2015**, *137*, 592–595. (b) Cheng, C.; Hartwig, J. F. *Science* **2014**, *343*, 853–857.
- (9) Friedel–Crafts silylation of electron-rich arenes was also reported recently: (a) Chen, Q.-A.; Klare, H. F. T.; Oestreich, M. *J. Am. Chem. Soc.* **2016**, *138*, 7868–7871. (b) Ma, Y.; Wang, B.; Zhang, L.; Hou, Z. *J. Am. Chem. Soc.* **2016**, *138*, 3663–3666. (c) Bähr, S.; Oestreich, M. *Angew. Chem., Int. Ed.* **2017**, *56*, 52–59. (d) Yin, Q.; Klare, H. F. T.; Oestreich, M. *Angew. Chem., Int. Ed.* **2016**, *55*, 3204–3207. (e) Klare, H. F. T.; Oestreich, M.; Ito, J.-i.; Nishiyama, H.; Ohki, Y.; Tatsumi, K. *J. Am. Chem. Soc.* **2011**, *133*, 3312–3315.
- (10) (a) Toutov, A. A.; Liu, W.-B.; Stoltz, B. M.; Grubbs, R. H. *Org. Synth.* **2016**, *93*, 263–271. (b) Toutov, A. A.; Liu, W.-B.; Betz, K. N.; Stoltz, B. M.; Grubbs, R. H. *Nat. Protoc.* **2015**, *10*, 1897–1903. (c) Toutov, A. A.; Liu, W.-B.; Betz, K. N.; Fedorov, A.; Stoltz, B. M.; Grubbs, R. H. *Nature* **2015**, *518*, 80–84. (d) Fedorov, A.; Toutov, A. A.; Swisher, N. A.; Grubbs, R. H. *Chem. Sci.* **2013**, *4*, 1640–1645.
- (11) Banerjee, S.; Yang, Y.-F.; Jenkins, I. D.; Liang, Y.; Toutov, A. A.; Liu, W.-B.; Schuman, D. P.; Grubbs, R. H.; Stoltz, B. M.; Krenske, E. H.; Houk, K. N.; Zare, R. N. *J. Am. Chem. Soc.* **2017**, DOI: 10.1021/jacs.6b13032, (following paper in this issue).
- (12) Frisch, M. J.; Trucks, G. W.; Schlegel, H. B.; Scuseria, G. E.; Robb, M. A.; Cheeseman, J. R.; Scalmani, G.; Barone, V.; Mennucci, B.; Petersson, G. A.; Nakatsuji, H.; Caricato, M.; Li, X.; Hratchian, H. P.; Izmaylov, A. F.; Bloino, J.; Zheng, G.; Sonnenberg, J. L.; Hada, M.; Ehara, M.; Toyota, K.; Fukuda, R.; Hasegawa, J.; Ishida, M.; Nakajima, T.; Honda, Y.; Kitao, O.; Nakai, H.; Vreven, T.; Montgomery, J. A., Jr.; Peralta, J. E.; Ogliaro, F.; Bearpark, M.; Heyd, J. J.; Brothers, E.; Kudin, K. N.; Staroverov, V. N.; Keith, T.; Kobayashi, R.; Normand, J.; Raghavachari, K.; Rendell, J. M.; Burant, J. C.; Iyengar, S. S.; Tomasi, J.; Cossi, M.; Rega, N.; Millam, J. M.; Klene, M.; Knox, J. E.; Cross, J. B.; Bakken, V.; Adamo, C.; Jaramillo, J.; Gomperts, R.; Stratmann, R. E.; Yazyev, O.; Austin, A. J.; Cammi, R.; Pomelli, C.; Ochterski, J. W.; Martin, R. L.; Morokuma, K.; Zakrzewski, V. G.; Voth, G. A.; Salvador, P.; Dannenberg, J. J.; Dapprich, S.; Daniels, A. D.; Farkas, O.; Foresman, J. B.; Ortiz, J. V.; Cioslowski, J.; Fox, D. J. *Gaussian 09*, Rev. D.01; Gaussian, Inc.: Wallingford, CT, 2010.
- (13) (a) Lee, C.; Yang, W.; Parr, R. G. *Phys. Rev. B: Condens. Matter Mater. Phys.* **1988**, *37*, 785–789. (b) Stephens, P. J.; Devlin, F. J.; Chabalowski, C. F.; Frisch, M. J. *J. Phys. Chem.* **1994**, *98*, 11623–11627. (c) Becke, A. D. *J. Chem. Phys.* **1993**, *98*, 5648–5652. (d) Becke, A. D. *J. Chem. Phys.* **1993**, *98*, 1372–1377.
- (14) (a) Hariharan, P. C.; Pople, J. A. *Theor. Chim. Acta* **1973**, *28*, 213–222. (b) Hehre, W. J.; Ditchfield, R.; Pople, J. A. *J. Chem. Phys.* **1972**, *56*, 2257–2261. (c) Ditchfield, R.; Hehre, W. J.; Pople, J. A. *J. Chem. Phys.* **1971**, *54*, 724–728.
- (15) Zhao, Y.; Truhlar, D. G. *Theor. Chem. Acc.* **2008**, *120*, 215–241.
- (16) (a) Barone, V.; Cossi, M. *J. Phys. Chem. A* **1998**, *102*, 1995–2001. (b) Cossi, M.; Rega, N.; Scalmani, G.; Barone, V. *J. Comput. Chem.* **2003**, *24*, 669–681. (c) Takano, Y.; Houk, K. N. *J. Chem. Theory Comput.* **2005**, *1*, 70–77.
- (17) Ido, E.; Kakiage, K.; Kyomen, T.; Hanaya, M. *Chem. Lett.* **2012**, *41*, 853–854.
- (18) Given the rapid product formation, we were pleased to see no detectable entropy change in the reaction when monitored by calorimetry, even when conducted neat at 5 mmol scale. See SI for details.
- (19) We believe this trend may be explained by decreasing cation–anion interaction with larger cations.
- (20) Zhou, A.-X.; Mao, L.-L.; Wang, G.-W.; Yang, S.-D. *Chem. Commun.* **2014**, *50*, 8529–8532.
- (21) Hu, S.-W.; Wang, Y.; Wang, X.-Y.; Chu, T.-W.; Liu, X.-Q. *J. Phys. Chem. A* **2004**, *108*, 1448–1459.
- (22) (a) Bravo-Zhivotovskii, D.; Ruderfer, I.; Yuzefovich, M.; Kosa, M.; Botoshansky, M.; Tumanskii, B.; Apeloig, Y. *Organometallics* **2005**, *24*, 2698–2704. (b) Lucarini, M.; Marchesi, E.; Pedulli, G. F.; Chatgililoglu, C. *J. Org. Chem.* **1998**, *63*, 1687–1693.
- (23) (a) Schley, N. D.; Fu, G. C. *J. Am. Chem. Soc.* **2014**, *136*, 16588–16593. (b) Newcomb, M. *Tetrahedron* **1993**, *49*, 1151–1176.
- (24) For examples, see: (a) Chatgililoglu, C. *Acc. Chem. Res.* **1992**, *25*, 188–194. (b) Bennett, S. W.; Eaborn, C.; Hudson, A.; Jackson, R. A.; Root, K. D. *J. Chem. Soc. A* **1970**, 348–351.
- (25) (a) For a review, see: Sun, C.-L.; Shi, Z.-J. *Chem. Rev.* **2014**, *114*, 9219–9280. (b) Sun, C.-L.; Gu, Y.-F.; Wang, B.; Shi, Z.-J. *Chem. - Eur. J.* **2011**, *17*, 10844–10847. (c) Liu, W.; Cao, H.; Zhang, H.; Zhang, H.; Chung, K. H.; He, C.; Wang, H.; Kwong, F. Y.; Lei, A. *J. Am. Chem. Soc.* **2010**, *132*, 16737–16740. (d) Sun, C.-L.; Li, H.; Yu, D.-G.; Yu, M.; Zhou, X.; Lu, X.-Y.; Huang, K.; Zheng, S.-F.; Li, B.-J.; Shi, Z.-J. *Nat. Chem.* **2010**, *2*, 1044–1049. (e) Yanagisawa, S.; Ueda, K.; Taniguchi, T.; Itami, K. *Org. Lett.* **2008**, *10*, 4673–4676.
- (26) (a) Zhang, L.; Yang, H.; Jiao, L. *J. Am. Chem. Soc.* **2016**, *138*, 7151–7160. (b) Yi, H.; Jutand, A.; Lei, A. *Chem. Commun.* **2015**, *51*, 545–548.
- (27) (a) Barham, J. P.; Coulthard, G.; Emery, K. J.; Doni, E.; Cumine, F.; Nocera, G.; John, M. P.; Berlouis, L. E. A.; McGuire, T.; Tuttle, T.; Murphy, J. A. *J. Am. Chem. Soc.* **2016**, *138*, 7402–7410. (b) Barham, J. P.; Coulthard, G.; Kane, R. G.; Delgado, N.; John, M. P.; Murphy, J. A. *Angew. Chem., Int. Ed.* **2016**, *55*, 4492–4496. (c) Zhou, S.; Doni, E.; Anderson, G. M.; Kane, R. G.; MacDougall, S. W.; Ironmonger, V. M.; Tuttle, T.; Murphy, J. A. *J. Am. Chem. Soc.* **2014**, *136*, 17818–17826.
- (28) (a) Xu, L.; Zhang, S.; Li, P. *Org. Chem. Front.* **2015**, *2*, 459–463. (b) Cai, Y.; Roberts, B. P. *J. Chem. Soc., Perkin Trans. 1* **1998**, 467–476. (c) Chatgililoglu, C.; Scaiano, J. C.; Ingold, K. U. *Organometallics* **1982**, *1*, 466–469.
- (29) (a) Rendler, S.; Oestreich, M. *Synthesis* **2005**, *11*, 1727–1747. (b) Chuit, C.; Corriu, R. J. P.; Reye, C.; Young, J. C. *Chem. Rev.* **1993**, *93*, 1371–1448. (c) Holmes, R. R. *Chem. Rev.* **1996**, *96*, 927–950. (d) Corriu, R. J. P.; Perz, R.; Reye, C. *Tetrahedron* **1983**, *39*, 999–1009. (e) Boyer, J.; Corriu, R. J. P.; Perz, R.; Reye, C. *Tetrahedron* **1981**, *37*, 2165–2171.
- (30) Shekar, S.; Brown, S. N. *J. Org. Chem.* **2014**, *79*, 12047–12055.
- (31) Yang, D.; Tanner, D. D. *J. Org. Chem.* **1986**, *51*, 2267–2270.
- (32) (a) Corriu, R. J. P.; Guerin, C.; Henner, B.; Wang, Q. *Organometallics* **1991**, *10*, 2297–2303. (b) Corriu, R.; Guérin, C.; Henner, B.; Wang, Q. *J. Organomet. Chem.* **1989**, *365*, C7–C10.
- (33) The isolation of the pentacoordinate silicate was likely unsuccessful due to the instability of this species.
- (34) (a) Denmark, S. E.; Beutner, G. L. *Angew. Chem., Int. Ed.* **2008**, *47*, 1560–1638. (b) Couzijn, E. P. A.; Ehlers, A. W.; Schakel, M.; Lammertsma, K. *J. Am. Chem. Soc.* **2006**, *128*, 13634–13639.
- (35) Mitzel reported a redshift (from 2151 to 2107  $\text{cm}^{-1}$ ) of the trans Si–H stretching in *N,N*-dimethylaminopropylsilane [ $\text{H}_3\text{Si}(\text{CH}_2)_3\text{NMe}_2$ ] by IR, which is due to an attractive N–Si interaction to form a hypercoordinate complex as characterized by X-ray analysis: Hagemann, M.; Berger, R. J. F.; Hayes, S. A.; Stammli, H.-G.; Mitzel, N. W. *Chem. - Eur. J.* **2008**, *14*, 11027–11038.
- (36) We propose that this indicates the hydroxides are converted to the silanolates, and subsequently silicates, which serve as the active catalysts. See ref 17.
- (37) These trends are consistent with the reported pentacoordinate silicate hydrosilylation of ketones: Deiters, J. A.; Holmes, R. R. *J. Am. Chem. Soc.* **1990**, *112*, 7197–7202.
- (38) Kanabus-Kaminska, J. M.; Hawari, J. A.; Griller, D.; Chatgililoglu, C. *J. Am. Chem. Soc.* **1987**, *109*, 5267–5268.
- (39) Alternatively, given the precedent of pentacoordinate silicate serving as a single electron donor, a single electron transfer from **6** to  $\text{Et}_3\text{SiH}$ , followed by the evolution of  $\text{H}_2$  and generation of triethylsilyl radical, is also possible. See ref 32b.
- (40) Trimethylsilane is used as the hydrosilane to simplify calculations.

(41) Chisholm, M. H.; Drake, S. R.; Naiini, A. A.; Streib, W. E. *Polyhedron* **1991**, *10*, 337–345.

(42) (a) Postigo, A.; Kopsov, S.; Zlotsky, S. S.; Ferreri, C.; Chatgililoglu, C. *Organometallics* **2009**, *28*, 3282–3287. (b) Zaborovskiy, A. B.; Lutsyk, D. S.; Prystansky, R. E.; Kopylets, V. I.; Timokhin, V. I.; Chatgililoglu, C. *J. Organomet. Chem.* **2004**, *689*, 2912–2919.

(43) Sommer, L. H.; Ulland, L. A. *J. Am. Chem. Soc.* **1972**, *94*, 3803–3806.

(44) (a) Bottoni, A. *J. Phys. Chem. A* **1997**, *101*, 4402–4408. (b) Chatgililoglu, C. *Chem. Rev.* **1995**, *95*, 1229–1251. (c) Chatgililoglu, C.; Ingold, K. U.; Scaiano, J. C. *J. Am. Chem. Soc.* **1983**, *105*, 3292–3296.

(45) The bond energy of C–H bond in an ethyl radical is nearly a factor of 3 smaller than that of ethane: Blanksby, S. J.; Ellison, G. B. *Acc. Chem. Res.* **2003**, *36*, 255–263.

(46) (a) Honraedt, A.; Raux, M.-A.; Le Grogne, E.; Jacquemin, D.; Felpin, F.-X. *Chem. Commun.* **2014**, *50*, 5236–5238 (C2, C3 selectivity). (b) O'Hara, F.; Blackmond, D. G.; Baran, P. S. *J. Am. Chem. Soc.* **2013**, *135*, 12122–12134 (regioselectivity). (c) Roberts, B. P. *Chem. Soc. Rev.* **1999**, *28*, 25–35. (d) Cole, S. J.; Kirwan, J. N.; Roberts, B. P.; Willis, C. R. *J. Chem. Soc., Perkin Trans. 1* **1991**, 103–112.

(47) This type of proton abstraction usually requires polarity-reversal catalysis (PRC); see ref 46c.

(48) Murai, M.; Takeuchi, Y.; Yamauchi, K.; Kuninobu, Y.; Takai, K. *Chem. - Eur. J.* **2016**, *22*, 6048–6058.

(49) Fallon, T.; Oestreich, M. *Angew. Chem., Int. Ed.* **2015**, *54*, 12488–12491.

(50) Lu, B.; Falck, J. R. *Angew. Chem., Int. Ed.* **2008**, *47*, 7508–7510.

(51) (a) Sommer, L. H.; Korte, W. D.; Rodewald, P. G. *J. Am. Chem. Soc.* **1967**, *89*, 862–868. (b) Sommer, L. H.; Rodewald, P. G.; Parker, G. A. *Tetrahedron Lett.* **1962**, *3*, 821–824.

(52) Couzijn, E. P. A.; Slootweg, J. C.; Ehlers, A. W.; Lammertsma, K. *J. Am. Chem. Soc.* **2010**, *132*, 18127–18140. See also ref 28b.

(53) Sakurai, H.; Murakami, M.; Kumada, M. *J. Am. Chem. Soc.* **1969**, *91*, 519–520.

(54) (a) Sommer, L. H.; Ulland, L. A. *J. Org. Chem.* **1972**, *37*, 3878–3881. (b) Sakurai, H.; Murakami, M. *Chem. Lett.* **1972**, *1*, 7–8.

(55) (a) Toutov, A. A.; Betz, K. N.; Haibach, M. C.; Romine, A. M.; Grubbs, R. H. *Org. Lett.* **2016**, *18*, 5776–5779. (b) Weickgenannt, A.; Oestreich, M. *Chem. - Asian J.* **2009**, *4*, 406–410.

(56) Legault, C. Y. *CYLView*, 1.0b; Université de Sherbrooke, Canada, 2009; <http://www.cylview.org>.